

# **Equatorial Pacific 13° C Water Eddies in the Eastern South Pacific Ocean\***

**Gregory C. Johnson<sup>1,2</sup> and Kristene E. McTaggart<sup>1</sup>**

*for Journal of Physical Oceanography*

Submitted 29 May 2009

---

<sup>1</sup> NOAA/Pacific Marine Environmental Laboratory, 7600 Sand Point Way N. E.  
Bldg. 3, Seattle Washington 98115-6349, U.S.A.

<sup>2</sup> Corresponding author. Tel.: +1-206-526-6806; fax: +1-206-526-6744, E-mail  
address: [gregory.c.johnson@noaa.gov](mailto:gregory.c.johnson@noaa.gov) (G. C. Johnson).

\*PMEL Contribution Number 3334.

## *Abstract*

Argo float profile data are used to analyze warm, salty, weakly stratified, subthermocline eddies of tropical origin in the eastern subtropical South Pacific Ocean. These eddies contain anomalous signatures of the equatorial Pacific “13°C Water” that is carried poleward within the Peru-Chile Undercurrent (PCU) as it flows along the west coast of South America. From their eastern boundary origin the eddies spread westward and slightly northward, likely at least partly advected by the subtropical gyre. The eddy water properties contrast strongly with the colder, fresher, more strongly stratified waters of subantarctic origin being carried northward then westward by the gyre. Near the eddy source region, about 6% of Argo profiles sample eddies that are above selected thresholds for both salinity and potential vorticity anomalies relative to maps of the mean distributions of these properties on and around the core isopycnal for the eddies. The proportion of such profiles diminishes to about 1% near the northwestern limit of the eddy range, near 15°S and 115°W. These eddies are anticyclonic, with a subsurface radial velocity maximum near the core isopycnal for water property anomalies, hence a reduced surface expression. Their geostrophic signature sometimes extends below 1000 dbar, suggesting the eddies may influence float subsurface trajectories. Radial transports around the eddy centers are estimated to be on the order of  $2 \times 10^6 \text{ m}^3 \text{ s}^{-1}$  for the potential density layer  $26.0 < \sigma_\theta < 27.0 \text{ kg m}^{-3}$ , about the same magnitude as the poleward transport of the PCU.

# 1. Introduction

Eddies are ubiquitous features in the ocean, and their surface expression accounts for a significant fraction of variability in sea-surface height (Chelton et al. 2007). However, there are also subsurface eddies that may effect significant transfers of heat, freshwater, and other ocean properties. These eddies can be largely invisible at the sea surface. The anticyclonic lenses of warm, salty Mediterranean Outflow Water, or Meddies, found in the North Atlantic are a classic example of an eddy with a primarily subsurface expression (Richardson et al. 2000). Similar anticyclonic lenses composed of warm, salty Red Sea Outflow Water, or Reddies, are found in the Indian Ocean (Shapiro and Meschanov 1991). In addition, subsurface anticyclones of warm, salty, low potential vorticity water formed in the California Undercurrent (CU), or Cuddies, have been studied offshore of the west coast of North America (Simpson and Lynn 1990; Huyer et al. 1998; Garfield et al. 1999; Jerónimo and Gómez-Valdés 2007), and have even been observed as far east as Hawaii (Lukas and Santiago-Mandujano 2001).

Here Argo float data are analyzed to characterize striking anticyclonic subsurface lenses of warm, salty, weakly stratified water in the eastern South Pacific Ocean. The Argo sampling scheme (nominally  $3^\circ$  latitude  $\times$   $3^\circ$  longitude spacing between floats with a 10-day sampling interval) is not intended to resolve eddies. However, Argo floats report about 100,000 Conductivity–Temperature–Depth (CTD) profiles and 3,000 float-years of mid-depth displacements per year. These numerous data allow for analysis of serendipitously sampled ocean eddies, including the ones discussed here.

These eddies likely originate from the Peru-Chile Undercurrent (PCU). The PCU is a poleward-flowing eastern boundary undercurrent that carries warm, salty, oxygen-

poor, weakly stratified water of equatorial origin southward along the west coast of South America (Blanco et al. 2001). This water will here be referred to as Pacific Equatorial 13°C Water (TDW; Tsuchiya 1981), where 13°C indicates the temperature typical of a prominent thermocline (vertical stratification minimum) in the region. The PCU has a seasonal cycle, being strongest in the Austral spring and summer (Blanco et al. 2001) or spring and fall (Shaffer et al. 1999). Six years of velocity data at 220 m from a current meter mooring at the 875-m isobath at 30°S off Chile yields a mean alongshore velocity of  $0.13 \text{ m s}^{-1}$  to the south, suggesting a PCU transport on the order of  $1 \times 10^6 \text{ m}^3 \text{ s}^{-1}$  at that location (Shaffer et al. 1999). This transport estimate is similar to an estimate derived from CTD surveys at 10°S off Peru (Huyer et al. 1991), but variability about the mean is large in both cases.

The CU appears to share many characteristics with the PCU, including a subsurface, warm, salty, weakly stratified core of TDW, a narrow poleward subsurface flow along the coast of order  $0.1 \text{ m s}^{-1}$ , and a transport on the order of  $1 \times 10^6 \text{ m}^3 \text{ s}^{-1}$ , as well as temporal modulation in flow and water properties. The CU appears to shed anticyclonic eddies with subsurface cores, perhaps through baroclinic instabilities (Simpson et al. 1984; Lynn and Simpson 1990). Similarly, eastern boundary instabilities in the PCU, another poleward flowing undercurrent, could give rise to eddies. Whatever the dynamics of their origin, they then appear to propagate northwestward into the eastern subtropical South Pacific Ocean, where they are clearly observed by Argo floats.

Following this introduction, the data used in the analysis are discussed along with gridding and mapping routines (Section 2). Then results of the analysis are presented (Section 3). The paper ends with a discussion of the results (Section 4).

## 2. Data

CTD profile data collected by Argo floats are used in this study. Data collected from 1999 through February 2009 were downloaded from the Argo GCDAC in February 2009. Delayed-mode quality controlled data (adjusted values) are used where available. Otherwise, real-time quality controlled data (raw values) are used. Only data at pressures where pressure (P), temperature (T), and salinity (S) are all flagged as good (Argo quality flag 1) are retained in the analyses.

For geostrophic calculations, T and S data from each profile are linearly interpolated to a regular 10-dbar pressure grid, assuming that the shallowest good values of T and S are representative of surface values. Derived quantities are estimated from these vertically gridded values of P, T, and S. Contoured time-pressure sections of data from the floats are objectively mapped assuming a Gaussian covariance with decorrelation scales of 1 month and 50 dbar, and a noise-to-signal energy of 0.01.

Additionally, properties on potential density anomaly ( $\sigma_\theta$ ) surfaces are analyzed here. For this analysis, any derived parameters desired are calculated from the float P, T, and S data. Then, the measured and derived parameters are linearly interpolated to desired  $\sigma_\theta$  surfaces from each CTD profile used. The vertical distance over which interpolations are performed is retained for purposes of quality control.

Properties on isopycnals are mapped to a regular geographic grid using a loess smoother with a nominal zonal scale of 1000 km and a nominal meridional scale of 500 km. If there are fewer than 2000 points inside the ellipse with these radii, the scales are increased, retaining their proportionality, until the ellipse contains at least 2000 points. At each point on this grid, data within range of the smoother from that point are subject to

the following screens: First, data interpolated over too large a pressure interval are discarded. The discard thresholds range linearly from an interpolation interval exceeding 22 dbar at an interpolated pressure of 0 dbar to an interpolation interval exceeding 67 dbar at an interpolated pressure of 300 dbar. At interpolated pressures greater than 300 dbar, the discard threshold remains constant at an interpolation interval exceeding 67 dbar. Second, interpolated values that are more than three times the interquartile range from either the first or third quartiles are discarded. Finally, the filter-weighted center of the data is also calculated for each map. If its position is more than 1/3 of the distance from the center relative to the range of the smoother, the mapped data point is discarded as being too far from the data.

### **3. Results**

Here we discuss an individual eddy sampled by a single float using time-pressure sections of water properties and potential-temperature salinity ( $\theta$ -S) curves. We then put the eddies into context by discussing the large-scale circulation and mean water-property distributions on and around the core density of the eddies. We follow with an analysis of eddy anomalies from those mean water-property distributions. Finally, we analyze indications of eddy motion in float displacements as well as the geostrophic flow field associated with the eddies.

#### *An example eddy*

The eddies studied here are often obvious in time-pressure sections of water properties for individual floats. One example was sampled during profiles 48 and 50–52

(11 June – 23 July 2007) by the Argo float with WMO (World Meteorological Organization) ID 3900556 (Fig. 1). While sampling this eddy, the float was located near 24°S, 103°E, roughly 1000 km northeast of Easter Island (Fig. 2).

The time-pressure salinity section for 2007 from this float shows a salty lens with values exceeding 34.7 PSS-78 relative to a background of 34.4 (Fig. 1a). The anomalously salty values are strongest for  $300 < P < 500$  dbar ( $26.2 < \sigma_\theta < 26.7$  kg m<sup>-3</sup>) with a core near 350 dbar ( $\sigma_\theta \sim 26.5$  kg m<sup>-3</sup>). A similar section for potential temperature (Fig. 1b) shows a strong thermostad for  $11 < \theta < 12^\circ\text{C}$  (still in the range of the TWD thermostad, which can be colder than  $13^\circ\text{C}$ , especially in the eastern equatorial Pacific) coincident with the salinity anomaly, with clearly warmer water along  $\sigma_\theta = 26.5$  kg m<sup>-3</sup> during sampling of the eddy. As would be expected from the sections, the  $\theta$ - $S$  curves for the profiles in the eddy are anomalously warm and salty for  $26.2 < \sigma_\theta < 26.7$  kg m<sup>-3</sup> with respect to those for the other profiles collected by this float during 2007 (Fig. 3). Again, the core of the anomaly is seen at  $\sigma_\theta = 26.5$  kg m<sup>-3</sup> in  $\theta$ - $S$  space.

Isotherms, isopycnals, and isohalines all exhibit downward deflections below the core of the eddy for the example shown (Fig. 1) to pressures of almost 1200 dbar. Above the eddy core isopleths bow up to pressures as shallow as 150 dbar. There are two consequences of this pattern. First, the core of the eddies have anomalously weak stratification with planetary potential vorticity ( $\Pi = f/\rho \partial\rho/\partial z$ ) closer to zero than outside the eddy (Fig. 1c) but slightly stronger stratification at depths well below the core of the eddy compared to the background. In this instance, the core of the eddy under examination has values of  $\Pi > -25 \times 10^{-12} \text{ m}^{-1} \text{ s}^{-1}$ , compared with  $\Pi \sim -300 \times 10^{-12} \text{ m}^{-1} \text{ s}^{-1}$ . There are also values of  $\Pi < -200 \times 10^{-12} \text{ m}^{-1} \text{ s}^{-1}$  near 500 dbar compared with

surrounding values of  $\Pi > -100 \times 10^{-12} \text{ m}^{-1} \text{ s}^{-1}$  at the same pressure. However, these more strongly stratified waters below the core are not so anomalous in isopycnal coordinates, since isopycnals undergo significant downward excursions below the eddy core, for instance on  $\sigma_\theta = 26.7 \text{ kg m}^{-3}$ . The second consequence of the isopycnal deflections above and below the eddy cores is an anticyclonic circulation around the eddies, with a subsurface maximum near their cores. Velocities (or more accurately transports per unit depth) associated with the eddies will be analyzed in more detail below.

#### *Large-scale subthermocline circulation and water-property distributions*

Maps of the acceleration potential and  $S$  on  $\sigma_\theta = 26.5 \text{ kg m}^{-3}$  (Fig. 4a,b) and  $\Pi$  for the layer  $26.2 \leq \sigma_\theta \leq 26.7 \text{ kg m}^{-3}$  (Fig. 4c), near and around the eddy cores, illustrate the equatorial origin of the eddies, and the higher latitude origins of the waters with which the eddy signatures contrast so strongly. Acceleration potential on  $\sigma_\theta = 26.5 \text{ kg m}^{-3}$  referenced to 900 dbar reveals the subsurface expression of the subtropical gyre. On this isopycnal the gyre axis where interior flow is primarily northward is located from 25–30°S. South of the axis there is eastward flow to at least 40°S, with some perturbations around New Zealand. North of the axis the flow is mostly westward. However, there is a trough in acceleration potential outlined by the 1.16 geopotential meter contour that runs from about 5°S in the western Pacific to 20°S west of South America. North of this trough the flow is mostly eastward, with an increasingly southward component approaching South America. This flow appears to extend southward along the west coast of South America to about 25°S. This eastward flow near the equator is the southern subsurface countercurrent (SSCC), or Tsuchiya Jet (Tsuchiya 1972), which brings warm,



salty, weakly stratified (hence low  $\Pi$ ) TDW eastward and then southward in the PCU (Johnson and McPhaden 1999; Blanco et al. 2001). Note that here acceleration potential on  $\sigma_\theta = 26.5 \text{ kg m}^{-3}$  is referenced to 900 dbar primarily because some of the float profiles only reach to 1000 dbar or so, so a 900-dbar zero velocity surface uses data from more floats than would a deeper reference level. Analysis of float displacement data at 900 dbar (Davis 2005) demonstrates that accounting for the flow field at that depth would increase the strength of the circulation over that shown here, but not change the general pattern or directions of flow inferred.

The salinity (Fig. 4b) and potential vorticity (Fig. 4c) fields on and around  $\sigma_\theta = 26.5 \text{ kg m}^{-3}$  respectively are remarkably similar in pattern and reflect the influence of at least three different water masses. A tongue of relatively salty, (warm), and low magnitude  $\Pi$  waters of subtropical origin centered near 35°S at 170°W and 30°S at 140°W spreads eastward along the easterly flow in the southern part of the subtropical gyre. Near the southeastern edge of the mapped region very fresh, (cold), and high magnitude  $\Pi$  water of subantarctic origin is swept northward and then westward in the subtropical gyre. Finally, a tongue of salty (outlined by the 34.9 isohaline at about 5°S in the western Pacific), (warm), and low magnitude  $\Pi$  equatorial water (TDW) is swept eastward in the SSCC and then increasingly poleward approaching South America. There are strong lateral gradients of  $S$ , (hence  $\theta$ ), and  $\Pi$  between the subantarctic influences moving equatorward and then westward in the subtropical gyre, and the equatorial influences moving eastward near the equator and then southward along the west coast of South America. It is this contrast that allows the TDW eddies to stand out when they drift westward into more subantarctic waters, and also raises the possibility

that they may mix substantial amounts of equatorial water properties into the subantarctic ones found along the eastern flank of subthermocline subtropical gyre.

### *Eddy distribution and water-property statistics*

Locating the eddies in individual profiles is somewhat subjective and not easy to do definitively in a reproducible fashion. Here we have chosen to use  $S$  and  $\Pi$  anomalies (referred to as  $S_a$  and  $\Pi_a$ ) on  $\sigma_\theta = 26.5 \text{ kg m}^{-3}$  as an objective criteria for locating float profiles taken in an eddy. To estimate these anomalies the mapped values of these properties interpolated to the spatial location of each profile are subtracted from the values of these properties from each profile vertically interpolated to the isopycnal. Hence eddies should be salty, (warm), and positive in  $\Pi$  (lower in magnitude, and so closer to equatorial values, but remember that  $\Pi$  is negative in the southern hemisphere) with respect to the background. After some experimentation we settled upon a requirement for  $S_a > 0.15$  and  $\Pi_a > 75 \times 10^{-12} \text{ m}^{-1} \text{ s}^{-1}$  on and around this isopycnal, respectively, for a given profile to be identified as sampling an eddy. These are both 1.5 times the contour interval for the large-scale maps of properties on or around  $\sigma_\theta = 26.5 \text{ kg m}^{-3}$  (Fig. 2), hence require that the profiles identified as sampling eddies have properties typical of the mean fields at least a few hundred km eastward and/or northward of their location.

With these criteria (adding the criterium that  $|S_a| < 0.1$  on  $\sigma_\theta = 27.2 \text{ kg m}^{-3}$ , an isopycnal with relatively small lateral gradients, to exclude real-time data from floats reporting potentially problematic salinity values), a total of 227 profiles sampling eddies are found in a geographically limited area of the southeast Pacific subtropical gyre, all

westward and southward of  $S = 34.7$  on  $\sigma_\theta = 26.5 \text{ kg m}^{-3}$ , and east of  $115^\circ\text{W}$  (Fig. 2). A visual examination of all the eddies showed this potential isopycnal to be close to the core of almost all of them.

The better to examine the prevalence and characteristics of these eddies, an admittedly arbitrary area containing them is selected (Fig. 2). The area is bounded to the east by South America, to the north by  $S = 34.7$  on  $\sigma_\theta = 26.5 \text{ kg m}^{-3}$ , to the west by  $\sim 115^\circ\text{W}$ , and to the south by a line segment between  $115^\circ\text{W}$ ,  $20^\circ\text{S}$  and  $90^\circ\text{W}$ ,  $40^\circ\text{S}$  and another line segment from there along  $40^\circ\text{S}$  to South America. There are 227 profiles from 31 floats sampling eddies out of 7920 profiles from 123 floats that passed the quality control criteria within this local region. In other words, nearly 3% of the profiles within the region sample an eddy strong enough to pass the objective criteria.

The sparse data coverage around  $25^\circ\text{S}$  in some of the study region prevents construction of a satisfactory map of eddy concentration, but the plot of eddy locations suggests they are more prevalent to the south and east, and rarer to the north and west, consistent with an origin in the PCU near the South American Coast (Fig. 2). Binning the fraction of profiles sampled by eddies relative to the total number of profiles in  $10^\circ$  latitude or  $8^\circ$  longitude bins (not shown) confirms this impression by quantifying that the eddies are more prevalent in the southeast and rarer in the northwest end of this region. The fraction of floats sampling eddies within the region selected in  $10^\circ$  longitude bins rises from 1% in the western end of the region to as high as 6% in the eastern end. Eddies are also more prevalent to the south, with regional fractions in  $8^\circ$  latitude bins rising from 2% near their northern limits to about 5% near their southern limits.

Some of the floats sample eddies, or presumably the same eddy, several times in a row, and sometimes they only sample an eddy in a lone profile. Again, it is difficult to discern one eddy from another, but there are 68 distinct series of consecutive cycles of profiles from floats sampling eddies based on the anomaly criteria above. If multiple floats sample one eddy, this number may be an overestimate of the number of eddies sampled. If the floats move out of an eddy for one profile, or the anomaly values dip below the threshold criteria for one profile, but then the float resumes sampling the same eddy, that may also tend to make the number an overestimate of the number of eddies sampled.

The eddies comprise a tail of highly correlated positive  $\Pi_a$  and  $S_a$  values in a bivariate census of these properties (Fig. 5) around the eddy core density for all the profiles within this local region. This census unsurprisingly reveals a distribution peaked at zero anomaly for both properties. The eddies comprise a relatively small portion of the total profiles in this region. However, the distribution of  $S$  and  $\Pi$  is clearly skewed towards salty and low magnitude values by their presence. This result supports the assertion that the eddies are a source of warm, salty, weakly stratified water of equatorial origin within the region. It also illustrates that they are relatively rare within the region, and why they might not be often observed by sparse ship-based measurement programs.

#### *Eddy motion and rotational circulation*

The floats that sample multiple consecutive profiles within an eddy (or eddies) appear to drift mostly a bit north of west. This impression is confirmed by examining the mean displacement of floats between consecutive profiles sampling eddies according to

the objective anomaly criteria. This strategy yields 159 displacement vectors with a mean amplitude of  $0.021 \text{ m s}^{-1}$  oriented towards  $291^\circ\text{T}$  ( $21^\circ$  north of west). Principal component analysis yields a nearly circular variance ellipse, which, assuming each displacement is statistically independent, yields a 95% confidence limit estimated to be  $0.006 \text{ m s}^{-1}$ . Thus, the eddies appear to be drifting mostly north of west in a statistically significant manner. This interpretation is consistent with advection away from a source off the South American coast roughly in the direction of the mean flow field (Fig 3; Fig. 4a). Eddies will also propagate westward on a  $\beta$ -plane even in the absence of a background flow (McWilliams 1985).

It is possible that the floats are simply drifting northwestward through stationary features or sampling multiple eddies on consecutive cycles. After all, their mean drifts are mostly characteristic of the mean flow at their 1000-dbar parking pressure (Davis 2005), and not the core of the much shallower eddies at  $\sigma_\theta = 26.5 \text{ kg m}^{-3}$ . However, in a few instances the floats collect consecutive profiles in eddies over a distance of a few hundred kilometers, a large lateral scale for a vertically confined feature (McWilliams 1985). In addition, sometimes the eddies exhibit geostrophic shear signatures that penetrate to 1000 dbar or deeper, and so may influence the float trajectories.

One way to quantify the dynamic signature of these eddies would be to compute the geostrophic velocities between a profile within the eddy core and one or more surrounding profiles typical of conditions outside the eddy. Determining a distance to use between profiles for this calculation is somewhat problematic, since there are nominally ten days between Argo profiles, and an eddy propagating at only a few centimeters per second would move tens of kilometers over that time interval. Forgoing

dividing by a distance between profiles during a geostrophic calculation yields a transport per unit depth instead of velocity, perhaps a more relevant property.

For the example eddy sampled by Argo float WMO ID 3900556, referencing the geostrophic calculations to the deepest common level (1975 dbar) among profile 50 (the profile with the strongest eddy signatures, identified by visual inspection) and each of profiles 45, 46, 53, and 54 (two profiles taken before the eddy was sampled and two more after the eddy was sampled, again identified by visual inspection) yields 4 profiles of estimated transport per unit depth for the eddy. The mean and standard deviation of these estimates at each pressure (Fig. 6) suggest that the shear signature for this particular eddy extends as deep as 1200 dbar. The peak mean geostrophic transport per unit depth exceeds  $10,000 \text{ m}^2 \text{ s}^{-1}$  at 360 dbar, with values decaying toward zero in a nearly Gaussian manner above and below that pressure. The eddy apparently has a surface expression about half that of its peak subsurface dynamical signature. However, the variance in the upper ocean geostrophic estimates is large, probably owing to the variety of other phenomena sampled by the profiles in the upper ocean, including the passage of almost a full season of the annual cycle (Fig. 1).

Such geostrophic transport estimates require identification of profiles within the core of each eddy, as well as profiles typical of the interior of each eddy. We visually inspected all of the available float time-series in the region and identified 87 eddies with cores inside the study region. Some of these eddies have signatures that are below the threshold for automated detection (hence the greater number here than the 68 identified by the automated method), but are clearly eddies nonetheless. For each eddy a core profile was identified along with up to two pairs of profiles devoid of eddy signal (that is

to say, typical of the ambient surroundings). The first pair was chosen to be as close to immediately before the eddy was encountered as possible and the second pair immediately after the float stopped sampling the eddy. Sometimes it was not possible to choose so many exterior profiles, such as when the eddy was sampled at the beginning or end of the float time-series. Often there were intervening profiles between the core and exterior profiles where the eddy signal was weaker, but those are ignored in the transport estimates made here.

Here we limit further analysis of transports around the eddies to the layer  $26.0 < \sigma_\theta < 27.0 \text{ kg m}^{-3}$ , which roughly encompasses the warm salty water of tropical origin, with the denser limit approaching the salinity minimum of Antarctic Intermediate Water and the lighter limit around the salinity minimum often found at the base of the central waters. This layer is easily compared with PCU transport estimates that have sometimes been made over a similar density interval. In addition, it avoids the mixed layer and some of the upper water column, where the seasonal cycle can be aliased into transport estimates. The deepest common level (generally near 1000 or 2000 dbar) for each eddy core and its surrounding profiles is used for a zero-velocity surface. The 87 profiles visually identified as being within the eddy cores and accompanying sets of profiles outside these cores allow 330 volume transport estimates for the density layer given above (Fig 7), which yield a mean (and standard deviation) of  $2.3 (\pm 1.5) \times 10^6 \text{ m}^3 \text{ s}^{-1}$ . (For the example from Argo float WMO ID 3900556 discussed above the transport values are  $1.9 (\pm 1.3) \times 10^6 \text{ m}^3 \text{ s}^{-1}$ .) The median of  $2.1 \times 10^6 \text{ m}^3 \text{ s}^{-1}$  and the mode around  $1.25 \times 10^6 \text{ m}^3 \text{ s}^{-1}$  of the 330 transport estimates are both less than the mean, because the mean is skewed upward by a few high values, the maximum of which is  $7.9 \times 10^6 \text{ m}^3 \text{ s}^{-1}$ .

Of course, the cyclostrophic term can also play a significant role in the dynamical balance within eddies, suggesting examination of the gradient flow that accounts for curvature in the velocity field. The larger the velocity and the smaller the radius of the eddy, the more important that term will be. For anticyclonic eddies, including the cyclostrophic term tends to increase the velocity relative to the geostrophic estimate. The actual impact of the cyclostrophic term is impossible to assess, as the true radius of curvature for the velocity estimates presented here is unknown. However, assuming the radius of curvature is equal to the distance separating profiles provides some measure of the potential importance. For the transport estimates made here, 80% see less than a 5% increase in transport for the density layer in question when the curvature of the velocity field is included, and 95% see less than a 25% increase in transport. The true addition to geostrophic transports could be larger or smaller than that estimated here depending on the actual radii of curvature.

## **4. Discussion**

Anticyclonic subthermocline eddies with a warm, salty, weakly stratified core containing TDW are found in the eastern portion of the South Pacific subtropical gyre. They apparently originate in the poleward flowing PCU on the eastern boundary of the South Pacific and then spread west and north in the gyre. These eddies are observed in Argo float profile data, with the largest concentration (6% of profiles containing an eddy with both potential vorticity and salinity anomalies rising above set thresholds) closest to their source, tailing off to about 1% in the western and northernmost regions at which



profiles with these S and  $\Pi$  anomalies are found (115°W and 15°S). This distribution, together with the background flow field at the core isopycnal of the eddy, and the fact that floats sampling consecutive eddies tend to be drifting slightly north of west on average as they do so, all support this assertion.

The eddies discussed here have many similarities to Meddies and Cuddies. First, they likely derive from a subthermocline poleward flowing eastern boundary current consisting of anomalously warm, salty, and weakly stratified water. Secondly, their property cores and maximum azimuthal velocities are found below the thermocline, limiting their surface expression. Thirdly, they are predominantly anticyclonic (we found no cyclonic eddies in this region in our exploration). Fourthly, after forming they spread westward (and in the case of the South Pacific eddies slightly northward), contrasting strongly with ambient waters that are colder, fresher, and more stratified. Finally, they are a source of warmer, saltier, and more weakly stratified water in the subthermocline subtropical gyre.

The eddies are relatively infrequent away from their coastal generation region, amounting to only a few percent of profiles taken. Therefore, it is not very likely that even one would be seen in a single hydrographic section crossing the region where they are present. That fact, together with the fact that this region was very sparsely sampled prior to the advent of Argo, and that their dynamical surface expression is reduced from their subthermocline signature, means it is perhaps not surprising that we were unable to find a description of these eddies in the literature.

One could speculate as to the generation mechanism for these eddies. The fact that the azimuthal volume transport within the eddies for the layer  $26.0 < \sigma_\theta < 27.0 \text{ kg m}^{-3}$ ,  $\sim 2$

$\times 10^6 \text{ m}^3 \text{ s}^{-1}$ , is on the order of the volume transport of the PCU (Huyer et al. 1990; Shaffer et al. 1999; Leth et al. 2004) suggests they may be shed by some instability in the PCU. However, their exact generation region (whether large or small) can not be pinpointed using the Argo float data. Certainly abrupt changes in the orientation of the coastline or the steepness of the continental shelf could play some role in eddy generation through various instabilities. Poleward propagating coastal Kelvin waves may perturb the velocity field, triggering an eddy-generating instability.

Finally, these eddies may play a significant role in the distribution of water properties in the subtropical gyre. Clearly, they introduce some amount of warm, salty, low potential vorticity water into the much colder, fresher, more strongly stratified waters of subantarctic origin. The tropical waters injected so far south into the subtropical gyre by the eddies must modify mean property distributions there, analogous to the role of Meddies in creating a plume of warm and salty water into the mid-depth North Atlantic Ocean. However, to accurately estimate the property fluxes resulting from these eddies, one would need to know the rate at which the eddies are generated, their path, and the amount of anomalous water contained in each eddy. That information is unlikely to be garnered by Argo floats, but would require a more focused process study. Nonetheless, the Argo float data have been very useful in sampling these eddies, and allowing quantification of some aspects of their structure and distribution.

**Acknowledgments:** Float data used here were collected and made freely available by Argo (a pilot program of the Global Ocean Observing System) and contributing national programs (<http://www.argo.net/>). The NOAA Climate Program Office and the NOAA

Office of Oceanic and Atmospheric Research supported this research. The findings and conclusions in this article are those of the authors and do not necessarily represent the views of the National Oceanic and Atmospheric Administration. Discussions with John Lyman were helpful while writing this paper.

## Reference List

- Blanco, J. L., A. C. Thomas, M.-E. Carr, and P. T. Strub (2001) Seasonal climatology of hydrographic conditions in the upwelling region of northern Chile, *Journal of Geophysical Research*, 106, 11,451–11,467.
- Chelton, D. B., M. G. Schlax, R. M. Samelson, and R. A. de Szoeke (2007) Global observations of large oceanic eddies, *Geophysical Research Letters*, 34, L15606, doi:10.1029/2007GL030812.
- Davis, R. E. (2005) Intermediate-depth circulation of the Indian and South Pacific Oceans measured by autonomous floats. *Journal of Physical Oceanography*, 35, 683–707.
- Garfield, N., C. A. Collins, R. G. Paquette, and E. Carter (1999) Lagrangian exploration of the California Undercurrent, *Journal of Physical Oceanography*, 29, 560–583.
- Huyer, A., J. A. Barth, P. M. Kosro, R. K. Shearman, and R. L. Smith (1998) Upper-ocean water mass characteristics of the California Current, Summer 1993, *Deep-Sea Research II*, 45, 1411–1442.
- Huyer, A., M. Knoll, T. Paluskiewicz, and R. L. Smith (1991) The Peru Undercurrent: a study in variability, *Deep-Sea Research A*, 38, Suppl. 1, S247-S271.
- Jerónimo, G., and J. Gómez-Valdés (2007) A subsurface warm-eddy of northern Baja California in July 2004, *Geophysical Research Letters*, 34, L06610, doi:10.1029/2006GL028851.
- Johnson, G. C., and M. J. McPhaden (1999) Interior pycnocline flow from the subtropical to the equatorial Pacific Ocean, *Journal of Physical Oceanography*, 29, 3073–3098, doi:10.1175/1520-0485(1999)029<3073:IPFFTS>2.0.CO;2.

- Leth, O., G. Shaffer, and O. Ulloa (2004) Hydrography of the eastern South Pacific Ocean: results from the Sonne 102 cruise, May–June 1995, *Deep–Sea Research II*, 51, 2349–2369.
- Lynn, R. J. and J. J. Simpson (1990) The flow of the undercurrent over the continental borderland of Southern California, *Journal of Geophysical Research*, 95, 12,995–13,008.
- Lukas, R., and F. Santiago-Mandujano (2001) Extreme water mass anomaly observed in the Hawaiian Ocean Time Series, *Geophysical Research Letters*, 28, 2931–2934.
- McWilliams, J. C. (1985) Submesoscale, Coherent vortices in the Ocean. *Reviews of Geophysics*, 23, 165–182.
- Richardson, P. L., A. S. Bower, and W. Zenk (2000) A census of Meddies tracked by floats, *Progress in Oceanography*, 45, 209-250.
- Shapiro, G. I., and S. L. Meschanov (1991) Distribution and spreading of Red-Sea Water and salt lens formation in the northwest Indian-Ocean, *Deep-Sea Research A*, 38, 21-34.
- Shaffer, G., S. Hormazabal, O. Pizarro, and S. Salinas (1999) Seasonal and interannual variability of currents and temperatures off central Chile, *Journal of Geophysical Research*, 104, 29,951–29,961.
- Simpson, J. J., T. D. Dickey, and C. J. Koblinsky (1984) An offshore eddy in the California Current system, I, Interior dynamics, *Progress in Oceanography*, 13, 5-49.
- Simpson, J. J. and R. J. Lynn (1990) A mesoscale eddy dipole in the offshore California Current, *Journal of Geophysical Research*, 95, 13,009-13,022.

- Tsuchiya, M. (1972) A subsurface north equatorial countercurrent in the eastern Pacific Ocean, *Journal of Geophysical Research*, 77, 5981–5986.
- Tsuchiya, M. (1981) The origin of the Pacific Equatorial  $^{13}\text{C}$  Water, *Journal of Physical Oceanography*, 11, 794-812.

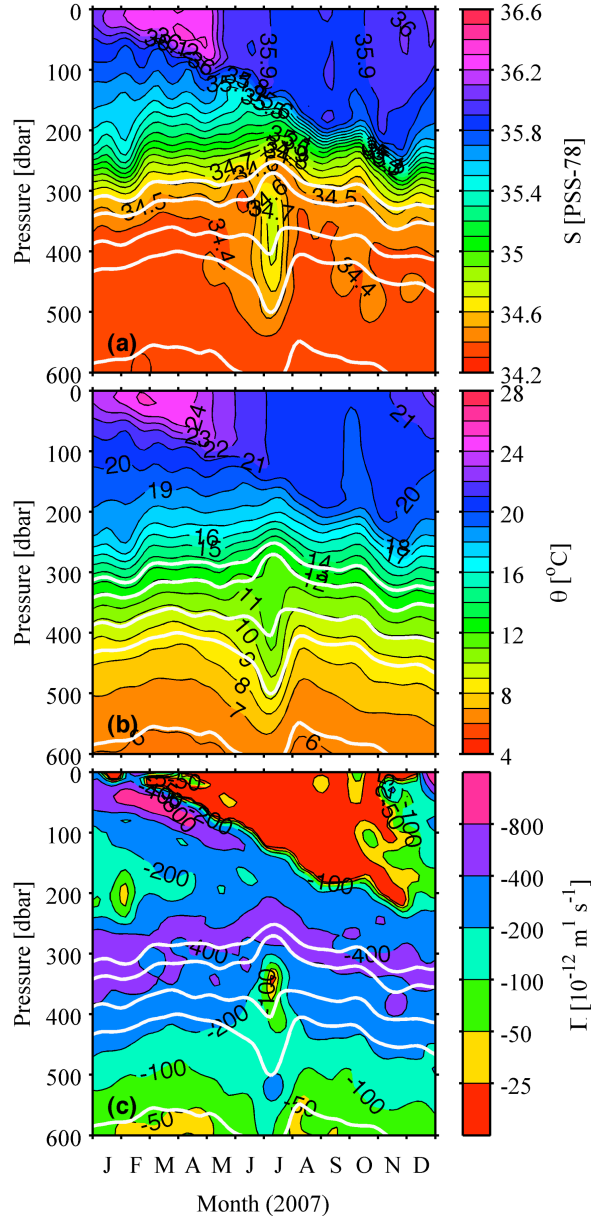


FIG. 1. Time-pressure sections of water properties during 2007 in the upper 600 dbar from Argo float WMO ID 3900556, located in the subtropical southeastern Pacific Ocean (see Fig. 2). (a) Salinity,  $S$ , contoured at 0.1 PSS-78 intervals, (b) potential temperature,  $\theta$ , contoured at 1 °C intervals, and (c) planetary potential vorticity,  $\Pi$ , contoured at doubling intervals from  $-25 \times 10^{-12} \text{ m}^{-1} \text{ s}^{-1}$  to  $-800 \times 10^{-12} \text{ m}^{-1} \text{ s}^{-1}$ . Contours for  $\sigma_\theta = 26.0, 26.2, 26.5, 26.7, \text{ and } 27.0 \text{ kg m}^{-3}$  are overlaid in white on each panel.

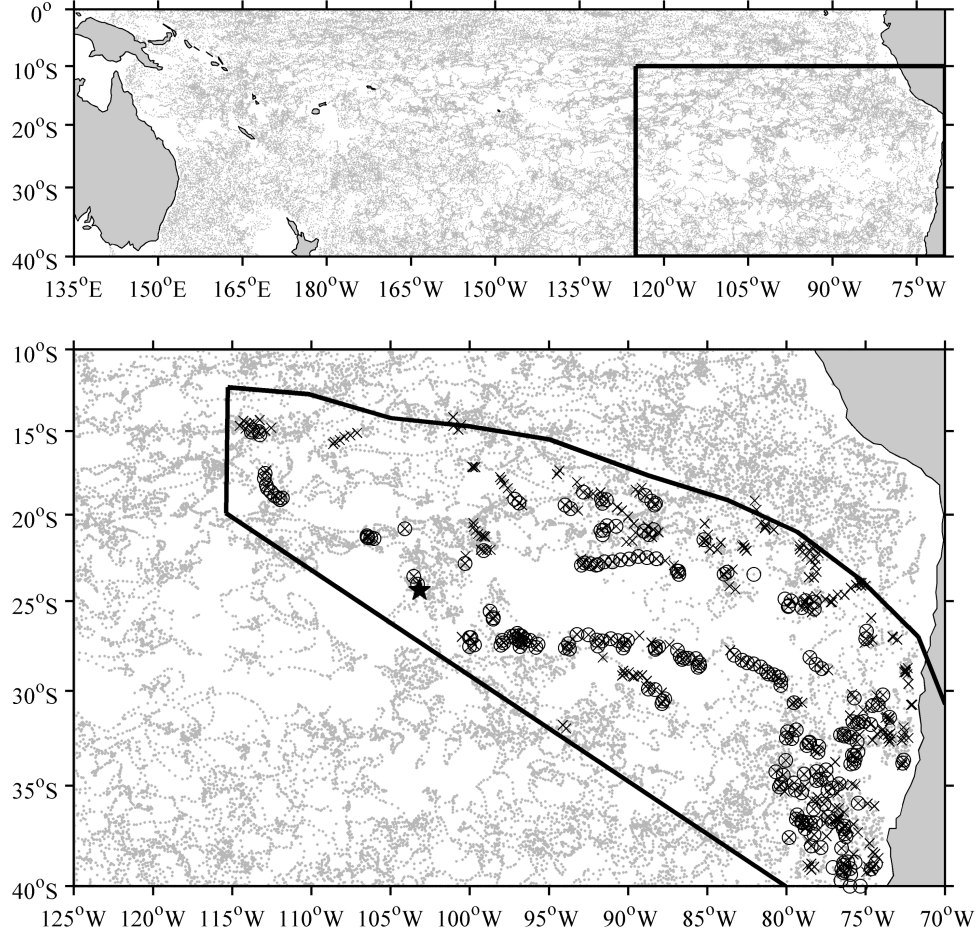


FIG. 2. Map of South Pacific (upper panel) with Argo float profiles (grey dots) used in this study and detail (lower panel; black lines on upper panel indicate geographic limits of lower panel) including the location of profile 50 from Argo float WMO ID 3900556 (solid black star), locations of other float profiles with eddies identified by salinity,  $S$ , and planetary potential vorticity,  $\Pi$ , anomaly criteria as discussed in the text (black circles), and eddies identified by visual inspection (black crosses). The region bounded to the east by South America, to the north by  $S = 34.7$  on  $\sigma_\theta = 26.5 \text{ kg m}^{-3}$ , to the west by  $\sim 115^\circ\text{W}$ , and to the south by a line segment between  $115^\circ\text{W}$ ,  $20^\circ\text{S}$  and  $90^\circ\text{W}$ ,  $40^\circ\text{S}$  and another from there along  $40^\circ\text{S}$  to South America (black lines on lower panel) is used to analyze local eddy statistics.



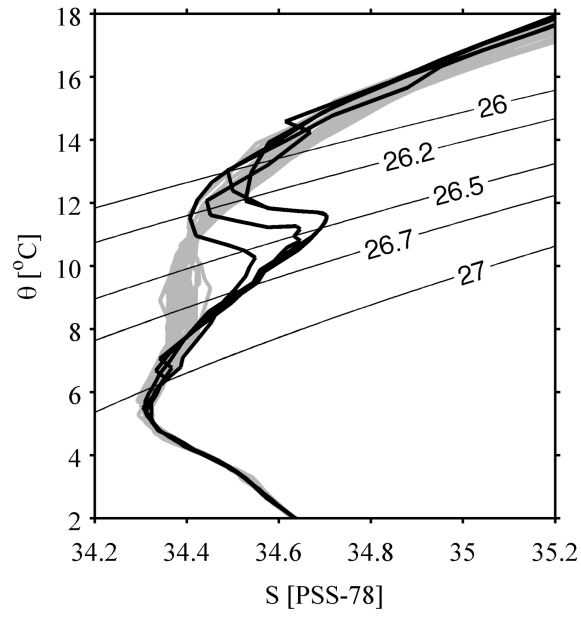


FIG. 3. Potential temperature–salinity ( $\theta$ – $S$ ) curves for all profiles taken in the subtropical southeastern Pacific Ocean during 2007 by Argo float WMO ID 3900556 (grey lines) highlighting profile numbers 48, 50–52 (black lines) with contours for  $\sigma_\theta = 26.0, 26.2, 26.5, 26.7$ , and  $27.0 \text{ kg m}^{-3}$ .

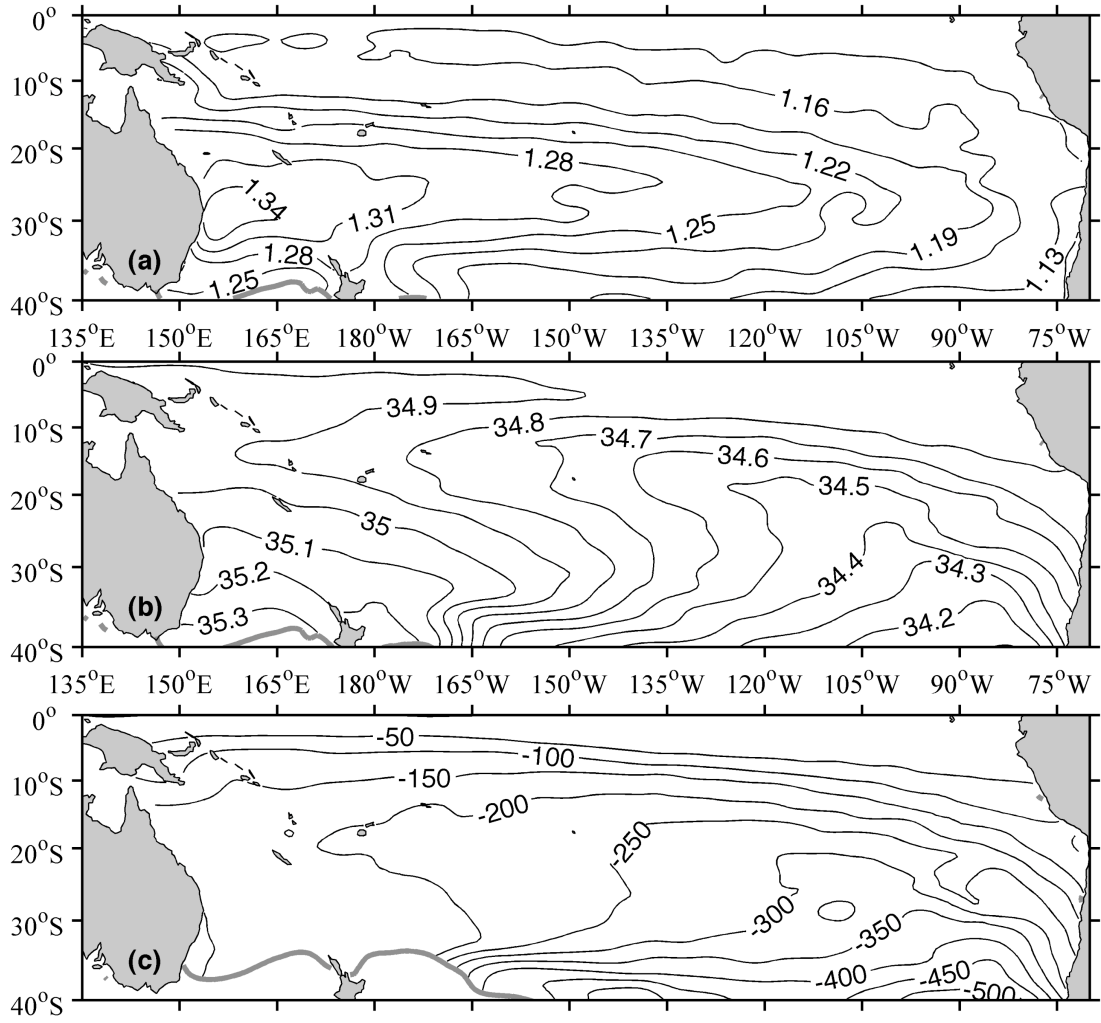


FIG. 4. Maps of mean South Pacific Ocean properties produced from Argo float data (Fig. 2) as described in the text. (a). Acceleration potential on  $\sigma_\theta = 26.5 \text{ kg m}^{-3}$ , relative to an assumed 900-dbar level of no motion, contoured at 0.03 geopotential meter intervals. (b). Salinity,  $S$ , on  $\sigma_\theta = 26.5 \text{ kg m}^{-3}$  contoured at 0.1 PSS-78 intervals. (c). Planetary potential vorticity,  $\Pi$ , estimated for the layer with  $26.2 \leq \sigma_\theta \leq 26.7 \text{ kg m}^{-3}$  contoured at  $50 \times 10^{-12} \text{ m}^{-1} \text{ s}^{-1}$ . Maps are masked where wintertime surface  $\sigma_\theta < 26.5 \text{ kg m}^{-3}$  in (a) and (b), and  $< 26.2 \text{ kg m}^{-3}$  in (c), with these southwestern locations outlined by a thick grey line.

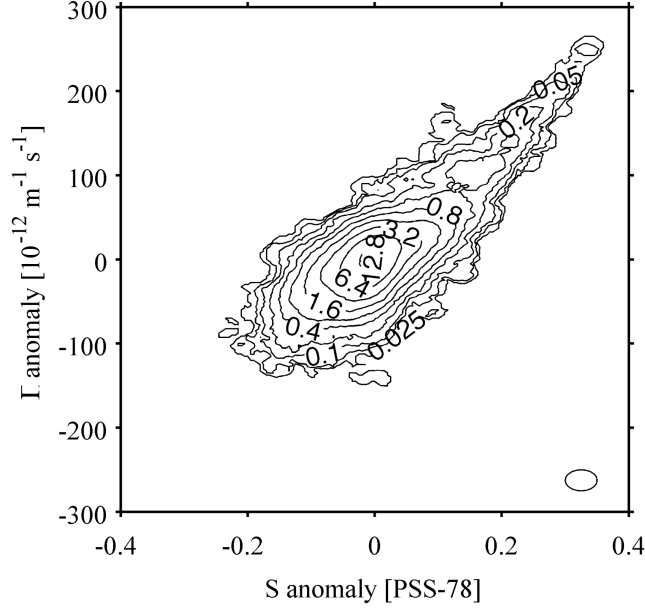


FIG. 5. Bivariate census of salinity anomalies,  $S_a$ , on  $\sigma_\theta = 26.5 \text{ kg m}^{-3}$  and planetary potential vorticity anomalies,  $\Pi_a$ , in the layer with  $26.2 \leq \sigma_\theta \leq 26.7 \text{ kg m}^{-3}$  for the Argo float profiles within a local region surrounding the eddies (Fig. 2, black line) that meet the quality control criteria discussed in the text. Percentages are counted in overlapping ellipsoidal bins with a  $S_a$  axis of 0.025 PSS-78 and a  $\Pi_a$  axis of  $12.5 \times 10^{-12} \text{ m}^{-1} \text{ s}^{-1}$  (representative ellipse shown in lower right hand corner). Contours of percentages start at 0.025% and double until reaching 12.8%.

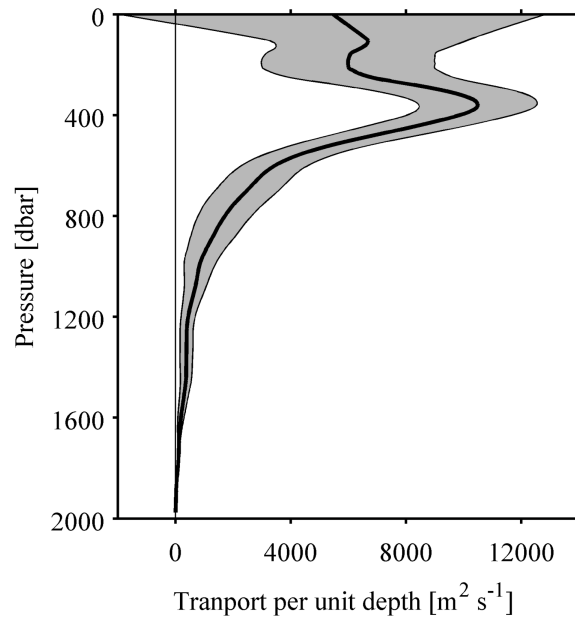


FIG. 6. Profile of transport per unit depth [ $\text{m}^2 \text{s}^{-1}$ , anticyclonic is positive] plotted versus pressure for the subsurface eddy of TDW for profile 50 of the Argo float with WMO ID #3900556. The geostrophic estimates reference geopotential anomaly profiles from the float to 1975 dbar. The mean (thick black line) of estimates made between profile 50 and each of profiles 45, 46, 53, and 54, is shown with a one standard deviation envelope (grey area).

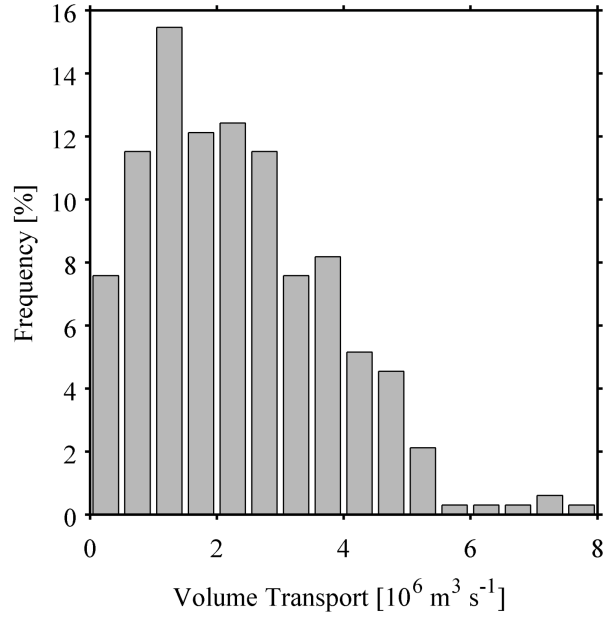


FIG. 7. Frequency of geostrophic volume transport [ $10^6 \text{ m}^3 \text{ s}^{-1}$ ] estimates within the potential density range  $26.0 < \sigma_\theta < 27.0$  between profiles identified as being within eddies (core profiles) and profiles identified as adjacent to the eddies. These estimates assume a zero-velocity surface at the deepest common pressure of each group of profiles associated with an eddy.